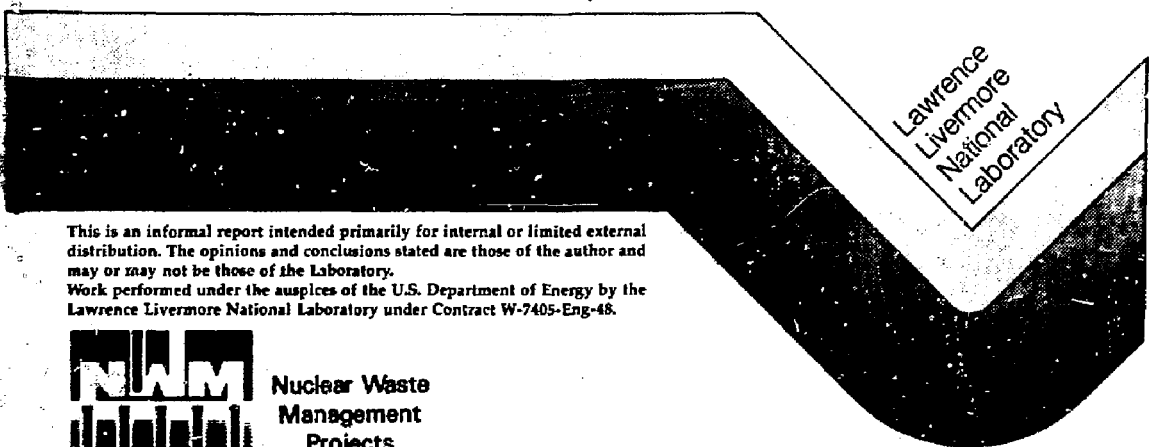UCID- 20412

PHYSICAL AND CHEMICAL CHANGES TO ROCK
NEAR ELECTRICALLY HEATED BOREHOLES
AT SPENT FUEL TEST-CLIMAX

J. M. Beiriger
W. B. Durham
F. J. Ryerson

January 1985

Nuclear Waste
Management
Projects

PHYSICAL AND CHEMICAL CHANGES TO ROCK NEAR ELECTRICALLY HEATED BOREHOLES AT SPENT FUEL TEST-CLIMAX[*]

J. M. Beiriger
W. B. Durham
F. J. Ryerson

ABSTRACT

Sections of Climax Stock quartz monzonite taken from the vicinity of two electrically heated boreholes at Spent Fuel Test-Climax (SFT-C) have been studied by scanning electron microscopy and optical microscopy for signs of changes in crack structure and in mineralogy resulting from operations at SFT-C. The crack structure, as measured by density of cracks and average crack lengths was found not to have changed as a result of heating, regardless of distance from the heater hole. However, rock near the heater borehole sampled in the north heater drift was found to be more cracked than rock near the borehole sampled in the south heater drift. Mineralogically, the post-test samples are identical to the pre-test samples. No new phases have been formed as a result of the test.

[*]This study was conducted as part of the Nevada Nuclear Waste Storage Investigations of the U.S. Department of Energy.

MASTER

INTRODUCTION

The recently concluded Spent Fuel Test-Climax (SFT-C) has tested, with an
in situ experiment, some of the concepts of an underground repository for
spent nuclear fuel (Ramspott et al., 1979). The present study is one of
several observational and laboratory studies in support of SFT-C aimed at
determining the combined and separate effects on rock of nuclear radiation,
heat, and mechanical load. The aim of this study is to determine the effect
on rock of heating alone.

The SFT-C is located in workings at the 420-m level below the surface in
the quartz monzonite portion of the Climax Stock at the Nevada Test Site. The
stock is unsaturated but not dry at this level. The water table is about
150 m below the test level. Canisters of spent nuclear reactor fuel were
emplaced in an array of boreholes, intermixed with boreholes containing
electrical simulators which duplicated the heat of the nuclear waste but not
the nuclear radiation (Figure 1). In the north and south heater drifts of
SFT-C additional electrical heaters were placed in 60-mm diameter boreholes to
provide thermal boundary conditions on the array of spent fuel canisters and
simulators. The rock near the electrically heated boreholes in the north and
south heater drifts were hotter than at any other location in the SFT-C
facility because the power output of the heaters was higher and because the
rock was nearer the heat source than was the case in the main array. It was
reasoned that if heat caused physical and chemical changes to any rock at
SFT-C, it would be most pronounced at the walls of these boreholes.

SAMPLE LOCATION

Pre- and post-test cores were taken from the vicinity of two of the electrical heater simulator boreholes: borehole five in the south heater drift, designated SHH5, and borehole ten in the north heater drift, NHH10. Three cores were taken from each borehole (Figure 2), one pre-test and two post-test. The pre-test core was simply the 25-mm-diameter core from the AX borehole made for the electrical heaters; their designations are those of the boreholes themselves: SHH5 and NHH10. Following the completion of testing operations at SFT-C and the removal of the heaters, a 150-mm-diameter core was taken approximately tangent to the heater borehole. This core was given the additional designation "PT" for "post-test". Core NHH10PT actually intersected the heater borehole, providing visual proof of the spatial relationship of pre- and post-test cores. Core SHH5PT barely grazed the heater borehole. The orientation of SHH5PT with respect to SHH5 was based on a fiduciary stripe made along the length of the core, and its distance from the wall of borehole SHH5 was calculated to be 3.7 mm based on measurements of core diameters and of the web between boreholes SHH5 and SHH5PT. The second post-test core, designated with an "A" suffix, was NX-size (45 mm outer diameter) and was cored parallel to, and at a radius of 760 mm from, each heater borehole.

The intervals of core which we sampled in this study were chosen to lie at a depth near the horizontal midplane of each 2.5 m-long heater, and at the same depth as one another, consistent with the retrievability of material. Thus, the sections used from cores SHH5, SHH5PT, and SHH5A all lay in the

4.05-m to 4.15-m interval. The sections from cores NHH10, NHH10PT, and NHH10A lay in the 4.18-m to 4.27-m interval. The exact relationship of these intervals to the positions of the heaters can be seen in core logs from the pre-test cores (Tewes, 1982).

The original reason to sample rocks from the vicinity of two different heater boreholes was to compare the effects to rock under different moisture conditions, given the potential physical and chemical changes heated water can bring about. In fact, the two heater boreholes we sampled may not be very different as regards water. Borehole SHH5 was cored into relatively dry rock (although dampness pervades the whole formation at this depth) and was located directly below a water-bearing shear zone which actively seeped water on the mine floor around SHH5. Borehole NHH10 intersected a major high angle structural feature known as the Receiving Room Fault, a broad, variably altered and clay-infilled zone roughly 4 m wide which also seeps water. The core log for NHH10PT confirms the intersection with the altered zone at depths surrounding the interval we sampled. The core log for NHH10A indicates the zone is more than a meter above the interval we sampled.

SAMPLE PREPARATION AND EXAMINATION TECHNIQUES

Sections of rock were prepared as polished sections for scanning electron microscopy (SEM) and as polished thin sections for optical microscopy (OM) and electron probe (EP) analysis. The polished sections and thin sections were prepared as matched facing pairs as shown in Figure 3. The cutting process went as follows: the core intervals were first sliced along vertical diametrical planes to reveal the face of interest. In the case of the "PT"

core, the slice was radial to the heater borehole; the azimuthal orientation of the slices in the other cores was arbitrary. Squares approximately 23 mm on a side were then cut from the faces of interest. Fourteen such squares were cut from the vicinity of each of the two heater boreholes (Figure 2): two from the pre-test core, ten from the "PT"-designated core, and two from the "A"-designated core. By the arrangement shown in Figure 2, the horizontal temperature gradient around each heater borehole was thus sampled twice, in parallel, adjacent rows. The locations of all 24 post-test sections are listed in Table 1.

In order not to confuse the twenty-eight pairs of sections as to their locations and faces of interest, various patterns of identifying notches were cut into the rock slabs as they were cut into squares. The notches also served to register facing SEM and OM sections. The cutting process was documented with color photographs, and all scrap material was retained, in order that petrographic features would serve as backup location identifiers.

Once all the squares had been cut, approximately 1 mm of material was ground from the faces of interest to remove cutting damage. Those faces were then ground flat with SiC powder in a sequence of steps from 240 to 1900 grit size. The sequence of steps shown in Figure 3 was then carried out.

Thin sectioning and polishing were carried out in standard petrographic fashion by Pacific Petro Labs, Mokelumme Hill, CA. Thin sections were 30 μm, thick and were polished to a 0.25-μm diamond finish. Cover slides were not attached. Note that because of the way in which we generated matched

pairs of sections, the thin section slices were supplied to Pacific Petro

already mounted on glass slides. The thick polished sections were polished to

a 1.0-µm diamond finish. They were not impregnated prior to polishing.

The thin sections were examined in the state received from Pacific Petro.

The thick sections were given further treatment to prepare them for SEM, as

prescribed by Sprunt and Brace (1974): The surfaces were first ion-milled

(argon ions, 7 kV accelerating voltage, 15° milling angle, 12 hour milling

time) to remove the remaining fine damage caused by mechanical polishing, then

were coated with a layer of carbon roughly 40 nm thick to prevent surface

charge buildup under the electron beam.

Crack counting techniques. For crack counting we used the rapid,

semi-automatic technique developed to measure subtle physical changes (i.e.

microfracturing) in Climax Stock quartz monzonite (CSQM) (Durham et al.,

1984). To avoid operator bias toward "interesting" areas, SEM photos were

taken at preassigned locations. Straight line "scans" were taken across each

section and micrographs were taken at 2-mm intervals along the scans.

Micrographs were taken at a magnification of 500X, using a solid-state under

quadrupole backscattered electron detector in the SEM. The cracks we counted

were only those considered "fresh" (sharp edges, no fill material, pieces fit

together; see Durham et al., 1984, for more detail). Our earlier studies

demonstrate that such "fresh" cracks include a significant background density

of cracks existing prior to operations at SFT-C. However, any new cracks

developed by such operations certainly fall in the "fresh" category. Grain

boundary cracks present a more ambiguous image in the SEM than intragranular

cracks mainly because of the obscurring contrast introduced by grain-to-grain chemical changes, and, as in the previous studies, were deliberately ignored in the interests of maintaining crack counting efficiency. The possible effect of ignoring grain boundary cracks in this study is analyzed under DISCUSSION below.

Microanalytical Techniques. Polished thin sections of all samples were examined in plane, cross-polarized, and reflected light in order to determine primary igneous and secondary phase mineralogy and textures. Subsequent to petrographic analysis the five samples from NHH10PT (numbers 1-5) were selected for microprobe analysis. The microprobe analyses were conducted with a 2 μm X 2 μm rastered beam at 15 na sample current (measured in a Faraday cup) with a 15 kV accelerating voltage. For each sample, 300 analyses were obtained along six, 50-point traverses per sample with a step interval of 400 μm. The data were sorted into mineral groups using stoichiometry and analytical totals as discriminants. After microprobe analysis, the samples were stained for plagioclase and K-feldspar and analyzed for modal abundances.

RESULTS

Crack Counting. Two scans were made across each of the 28 SEM sections, in the sequence given in Table 2. The first scan ran horizontally in the SFT-C coordinate system (i.e. radially from the heater borehole for the "PT"-designated sections), the second vertically. Eight to ten spots were counted on each scan (identification notches eliminated some of the spots). In all, 480 spots were photographed, and 1245 fresh cracks were identified and

measured (Table 3). Tables 4, 5, and 6 give the results: three crack parameters (described below) are given summarizing the measurements for each of the 28 SEM sections, and the tables are arranged to resemble the original geometrical arrangement of the sections. Additionally, Tables 4 and 5 give summary measurements for sections grouped by heater borehole.

The three crack parameters are areal number density of cracks in mm^{-2}, average length of individual cracks in μm, and areal total length density in mm/mm^2. The third parameter is exactly the product of the first two, but its presentation does serve a purpose. Firstly, it is calculated by a means other than simply taking the product of the first two parameters, thereby serving as a check of the calculations, and secondly it is usually the most sensitive of the three parameters since it has the combined sensitivity (and noise) of the first two parameters.

None of the three crack parameters is normally distributed, so the means and standard deviations given in Table 4, which were calculated on the basis of a normal distribution, are useful only for qualitative comparisons. Crack lengths turn out to be log-normally distributed (Figure 4) consistent with a similar finding by Weed and Durham (1982) on CSQM. The log-normal means and standard deviations for crack length given in Table 5 do allow quantitative statistical tests for trends. Neither crack number density nor total length density is log-normally distributed, also consistent with the findings of Weed and Durham (1982).

Table 6 gives detailed measurements for the horizontal traces only on the four "PT" sections closest to the heater holes (Figure 2, Table 1). Since the temperature gradient was strongest and since temperatures were highest along these four traces, trends might be expected to appear in the spot-to-spot data. Note that in Tables 4 and 5, such spot-to-spot detail is averaged across each section.

Petrography and Mineral Chemistry. Petrographic examination of post-test samples shows no differences between the samples from NHH1OPT and SHH5PT. Near both boreholes, the mineralogy compares favorably with that of the deuterically altered pre-test samples (Table 7). The samples are composed of a groundmass of subhedral grains of oscillatory zoned plagioclase, quartz, K-feldspar and biotite ranging from 0.5-2.0 mm in diameter. Common accessory phases include titanite (also present as an alteration product), allanite, zircon, and apatite. In the samples examined, quartz and K-feldspar phenocrysts up to 10 mm and 30 mm in diameter, respectively, are found.

In these deuterically altered samples, the hydrothermal alteration is found predominately on plagioclase and biotite within the groundmass. Plagioclase is altered to muscovite plus trace amounts of epidote and clinozoisite. The volume percentage of plagioclase altered is less than 5%. Biotite is altered to chlorite, epidote and titanite. In more intense alteration, muscovite may be present on biotite. In previous studies, it has been shown that intense alteration is localized near healed fractures which carried the hydrothermal solutions (Ryerson and Qualheim, 1983). The lack of intense alteration from NHH1OPT and SHH5PT is consistent with the absence of healed fractures in these samples.

A major finding of this work is that no additional phases have been formed as a result of heating at SFT-C. Due to this finding and the lack of any demonstrable difference between NHH1OPT and SHH5PT, additional analysis concentrated on the NHH1OPT samples.

Modal analyses of NHH1OPT samples are given in Table 7. An average from 19 deuterically altered samples from Connolly (1981) is given for comparison. The major variation among phases is between quartz, plagioclase and K-feldspar and is attributed to primary igneous processes (Ryerson and Qualheim, 1983). A plot of modal abundance versus distance from the heater indicates that no systematic variations in abundance exist with respect to heater position (Figure 5).

In order to assess the extent of ion exchange reactions which may have been produced during the test, feldspar analyses from the NHH1OPT samples are given in Table 8 and plotted versus distance from the heater in Figure 6. As shown for pre-test samples, the standard deviation among the plagioclase analyses is greater than that among the K-feldspars. This is attributed to primary igneous zonation (Ryerson and Qualheim, 1983). The compositions of these feldspars do not vary as a function of distance from the heater. Also the average composition of plagioclase and K-feldspar, 31.3% An and 89.7% Or, respectively, compares favorably with average compositions of all the samples from pre-test analysis, 31.2% An and 88.6% Or, respectively (Patrick et al., 1984).

DISCUSSION

Cast in the model of a normal distribution, the crack measurements show a great deal of scatter and two important "non-trends" (Table 4): 1) There is no systematic decrease in physical damage in the post-test core in the radial direction away from the heater boreholes, and 2) there is no apparent difference in crack structure between pre- and post-test core. The magnitude of the measurement scatter agrees very well with previous measurements on CSQM (Weed and Durham, 1982; Beiriger and Durham, 1984). The magnitudes of the three crack parameters are very close to those measured by the same operator under the same SEM conditions (Beiriger and Durham, 1984, passes B and C in their Table 4).

There is a strong suggestion that the crack structure is not the same in the vicinity of the two heater boreholes. Taking pre- and post-test core together (consistent with "non-trend" 2, above), the number density of cracks in the 14 sections from NHH10 appear higher than densities in the corresponding 14 section from SHH5. The averages over all 14 sections show 25% higher number density in NHH10 as compared with SHH5 (Table 4). It is intuitively difficult to ascribe the consistency of this trend to chance, but lacking a plausible distribution model for crack density, the probability of this trend being the result of random measurement fluctuation cannot be calculated. The average length of cracks near NHH10 is also higher (Table 5), and a statistical test can be applied here, since the distribution is log-normal. The t statistic for 1245 measurements is 1.970, meaning that in a two-tailed test (i.e. a difference of either sign) a random sampling of a

normal distribution will produce the observed difference on average one time

in 20. Combined with the qualitative inference based on crack density, this t

statistic provides a firm argument that the crack structure of core taken near

NHH10 is different from that of core taken near SHH5. A plausible explanation

of the longer and more populous cracks near NHH10 is the fact that 12 of the

14 sections examined from NHH10 (all but NHH10A-1 and -2) apparently fell

within the limits of the Receiving Room Fault (RRF). The hypothesis could be

tested by counting several hundred cracks from a few meters on either side of

the RRF. It is interesting to note that there is no macroscopic physical

evidence of the proximity to the RRF in the 90 mm lengths of core supplied to

us from NHH10 and NHH10PT. Thus our observations may support the phenomenon

frequently observed in laboratory test specimens that microfracturing is a

precursor to macroscopic failure.

There is a qualitative trend in the crack density in the NHH10PT core:

the measured density is higher towards the outer cylindrical surface of the

core (Table 4). The trend appears in both rows of sections in core NHH10PT

but does not appear in the average length measurement nor in any of the

measurements of core SHH5PT. The trend is interesting because Weed and Durham

(1982) saw a similar, albeit very poorly resolved, trend in another 150-mm

core from CSQM. A firm conclusion is beyond the capacity of the measurement

made so far. The coincidence, however, is noteworthy.

We have measured no physical damage to the host rock caused by the heater

hole environment. Does this imply that the rock in fact has suffered no

physical damage? There are a number of routes by which damage could have

escaped our detection. (1) Damage levels may be below our measurement resolution. In this case the effect on physical properties of the rock would probably also be small. (2) Cracks narrower than our practical resolution limit of 0.1 µm may exist. The effect of such cracks on physical properties depends on their density and geometrical arrangement, but the potential for important effects is not strong (See Kranz, 1983, for a review). If such cracks were caused by operations associated with SFT-C, it is possible that they were once wider in the presence of the high temperatures and gradients around the heater boreholes. It is, of course, possible that cracks seen now are wider than they were in situ, now that confining stresses have been relieved. (3) Damage was confined to grain boundary cracks. CSQM does exhibit loosened grain boundaries, but the number of such cracks is small. Roughly 1 crack in 5 is a grain boundary crack, based on a qualitative examination of photomicrographs used in our several crack counting studies. Grain boundary loosening appears in pre- and post-test core, and in rock which has been mechanically, rather than thermally, stressed. If confined to grain boundary cracks, the damage would be difficult to resolve quantitatively by direct observation. (4) Damage was manifested in some parameter (such as interconnectivity) which we did not measure. However, it is difficult to perceive how such damage could have occurred without affecting the density and/or length of intragranular cracks. (5) There is a remote possibility we have missed the forest for the trees, that is, the damage is concentrated in long cracks. In fact the maximum detectable crack length of a straight crack using our semi-automated technique is that of a long crack whose length is truncated at opposite corners of a micrograph, i.e., about 300 µm. This is probably the main cause of the slight departure of crack length distribution

from log-normality at longer lengths (Figure 4). Millimeter-scale and longer cracks are, in fact, plentiful in CSQM; they appear clearly in the low magnification mapping micrographs we take as part of the counting technique. However, such cracks appear in both the pre-and post-test sections with roughly the same frequency.

The strong detection of a difference in crack structure in two populations (NHH10 and SHH5) is unprecedented in the two previous studies using the semi-automated crack counting technique. Heretofore we found small, qualitative trends for which strong statistical support could not be generated. We have thus demonstrated that combined differences in crack density of the order of 25% (Table 4) and in average crack length of the order of 10% (Table 5) are detectable with a reasonable amount of effort.

No mineralogical changes due to hydration, dehydration or cation exchange reactions as a result of the test have been observed. If the wall rock was in contact with water during the test, then a number of the phases present should have been unstable. In fact, since the wall rock temperature was well in excess of $100^{\circ}C$, free water was driven off and some of the hydrous phases may also have been unstable. The absence of any reaction products indicates that the duration and intensity of the thermal maximum was not sufficient to overcome the activation barriers for these reactions, i.e. the kinetics were too sluggish.

CONCLUSIONS

Sections of Climax Stock quartz monzonite taken from the vicinity of
heater holes NHH10 and SHH5 at Spent Fuel Test-Climax (SFT-C) do not show any
change in their crack structure, as viewed by scanning electron microscope,
resulting from the in situ heating which occurred. In particular, rock
sampled at intervals along the temperature gradient away from the heater
boreholes shows, within measurement resolution, the same density of cracks and
average length of cracks as rock sampled before the heaters were powered up.

There is a significant difference from NHH10 to SHH5 in crack structure of
rock sampled in the vicinity of the heater holes. Rock near NHH10 has more
cracks per unit area (by roughly 25%), and its cracks have a longer average
length (by roughly 10%), than rock near SHH5. The augmented cracking near
NhH10 may be explained by the proximity of NHH10 to the Receiving Room Fault,
a major geological feature intersecting the mine workings at SFT-C.

Mineralogically, the post-test samples are identical to the pre-test
samples indicating the reaction kinetics for hydration, dehydration and cation
exchange reactions are too sluggish to be overcome by a test of this intensity
and duration.

REFERENCES

Beiriger, J. M., and W. B. Durham, SEM studies of stressed and irradiated
    Climax Stock quartz monzonite, University of California, Lawrence
    Livermore National Laboratory Report UCID-20052, 1984.

Connolly, J. A., Hydrothermal alteration in the Climax granite stock at the
    Nevada Test Site, M.S. Thesis, Arizona State University, Tempe, AZ., 1981.

Durham, W. B., J. M. Beiriger, and H. C. Weed, A rapid technique for counting
    cracks in rocks, Scanning Electron Microscopy, in press, 1984.

Kranz, R. L., Microcracks in rocks: A review, Tectonophys., 100, 449-480, 1983.

Patrick, W. C., T. R. Butkovich, R. C. Carlson, W. B. Durham, H. C. Ganow, G.
    L. Hage, E. J. Majer, D. N. Montan, R. A. Nyholm, N. L. Rector, F. J.
    Ryerson, H. Weiss, and J. L. Yow, Jr., Spent Fuel Test - Climax: Technical
    measurements interim report Fiscal Year 83, University of California,
    Lawrence Livermore National Laboratory Report UCRL-53294-83, 1984.

Ramspott, L. D., L. B. Ballou, R. C. Carlson, D. N. Montan, T. R. Butkovich,
    J. E. Duncan, W. C. Patrick, D. G. Wilder, W. T. Brough, and M. C. Mayr,
    Technical concept for a test of geologic storage of spent reactor fuel in
    the Climax granite at the Nevada Test Site, University of California,
    Lawrence Livermore National Laboratory Report UCRL-52796, 1979.

Ryerson, F. J. and B. J. Qualheim, Mineralogic and petrologic investigation of
    pre-test cores from Spent Fuel Test-Climax. University of California,
    Lawrence Livermore Laboratory Report UCID-19976, 1983.

Sprunt, E. S. and W. F. Brace, Direct observation of microcavities in
    crystalline rocks, Int. J. Rock Mech. Min. Sci., 11, 139-150, 1974.

Tewes, H. A., ed., Research results reported by OEO summer (1981) student
    employees of LLNL working with Earth Sciences (K) Division personnel,
    University of California, Lawrence Livermore National Laboratory Report
    UCID-19303, 1982.

Weed, H. C. and W. B. Durham, Drilling-induced borehole-wall damage at Spent
    Fuel Test-Climax, University of California, Lawrence Livermore National
    Laboratory Report UCID-19672, 1982.

TABLE 1:   Location of post-test sections
(Numbers give range of distance, in mm, to wall of heater hole)

NHH10			SHH5	
Section	Dist to wall of Heater Hole		Section	Dist. to wall of heater hole
NHH10PT-1, -6	0-22.5		SHH5PT-1, -6	4*-29
NHH10PT-2, -7	24-46		SHH5PT-2, -7	30-54
NHH10PT-3, -8	47-69	***	SHH5PT-3, -8	56-80
NHH10PT-4, -9	70-92		SHH5PT-4, -9	82-107
NHH10PT-5, -10	94-115		SHH5PT-5, -10	108-132
NHH10A-1, -2	760**		SHH5A-1, -2	760**

* $\pm$ 1 mm; all others $\pm$ 2 mm
** to center of section,
    $\pm$ 10 mm (est)
*** uncertainty progressive $\pm$ 0 to $\pm$ 2 mm

TABLE 2: Examination Sequence of SEM Sections

First Scan			Second Scan	
Sequence	Section		Sequence	Section
1	SHH5A-1		1	NHH10A-1
2	SHH5PT-5		2	NHH10PT-4
3	SHH5PT-4		3	NHH10PT-2
4	SHH5PT-3		4	NHH10-1
5	SHH5PT-2		5	SHH5PT-1
6	SHH5PT-1		6	SHH5PT-3
7	NHH10A-1		7	SHH5PT-5
8	NHH10PT-5		8	SHH5A-2
9	NHH10PT-4		9	SHH5PT-9
10	NHH10PT-3		10	SHH5PT-7
11	NHH10PT-2		11	SHH5-2
12	NHH10PT-1		12	NHH10PT-6
13	NHH10-1		13	NHH10PT-8
14	SHH5A-2		14	NHH10PT-10
15	SHH5PT-6		15	NHH10A-2
16	SHH5PT-7		16	NHH10PT-5
17	SHH5PT-8		17	NHH10PT-3
18	SHH5PT-9		18	NHH10PT-1
19	SHH5PT-10		19	SHH5-1
20	SHH5-2		20	SHH5PT-2
21	NHH10-2		21	SHH5PT-4
22	NHH10PT-6		22	SHH5A-1
23	NHH10PT-7		23	SHH5PT-10
24	NHH10PT-8		24	SHH5PT-8
25	NHH10PT-9		25	SHH5PT-6
26	NHH10PT-10		26	NHH10-2
27	NHH10A-2		27	NHH10PT-7
28	SHH5-1		28	NHH10PT-9

TABLE 3a: Number of Spots Photographed by Section*

								Totals, by Heater Hole
NHH10	18	17	19	17	17	17	17	239
	18	17	16	15	17	16	18	
SHH5	18	17	17	17	16	18	17	241
	17	17	17	17	17	18	18	

TABLE 3b: Number of Cracks Counted, by Section*

NHH10	58	52	54	24	27	71	41	693
	60	45	49	35	52	83	42	
SHH5	28	36	39	39	42	44	17	552
	37	43	69	42	31	36	49	

*Key to spatial arrangement of numbers in Tables 3-5 (arranged to resemble spatial arrangement of samples--see Figure 1)

NHH10	NHH10-1	NHH10PT-1	NHH10PT-2	NHH10PT-3	NHH10PT-4	NHH10PT-5	NHH10A-1
	NHH10-2	NHH10PT-6	NHH10PT-7	NHH10PT-8	NHH10PT-9	NHH10PT-10	NHH10A-2
SHH5	SHH5-1	SHH5PT-1	SHH5PT-2	SHH5PT-3	SHH5PT-4	SHH5PT-5	SHH5A-2
	SHH5-2	SHH5PT-6	SHH5PT-7	SHH5PT-8	SHH5PT-9	SHH5PT-10	SHH5A-1

TABLE 4: Crack Counting Results*
(Mean ± 1 std. dev., assuming informal distributions)

Density (number/mm²)

NHH10							Totals by Heater Hole
96+97 99±83	94+111 91±95	91+82 93±85	42+55 69±67	47+48 93±81	124+111 154±85	72+87 69±64	87+86
SHH5							
46+93 65±81	63+88 75±68	72+57 120±99	68+86 73±90	80+79 54±52	73+83 59±58	30+58 91±98	69+80

Average length (μm)

NHH10							
42+43 30±35	45+44 52±43	48+46 36±41	61+62 38±28	54+46 41±40	42+51 28±31	38+44 28±31	40+42
SHH5							
40+39 31±42	24+31 36±42	31+30 30±26	45+54 39±36	40+42 46±54	26+31 43±38	34+35 22±16	35+38

Length Density (mm/mm²)

NHH10							
4.00+3.28 2.97±3.00	4.05+5.29 3.94±4.50	4.07+3.76 3.24±3.93	2.54+3.53 2.66±2.66	2.57+3.55 3.79±3.80	5.20+4.88 4.32±1.97	2.74+2.39 1.91±2.22	3.46+3.64
SHH5							
1.85+2.57 1.98±2.81	1.54+2.39 2.67±2.58	2.19+2.10 3.65±2.90	3.03+3.35 2.85±3.44	3.11+3.67 2.51±2.51	1.90+2.15 2.55±2.96	0.66+1.20 2.75±3.22	2.38+2.79

*Table 3 gives key to arrangement of numbers

TABLE 5. Average Length of Cracks*
(Mean $\pm$ 1 std. dev. of $\log_e$[average crack length in μm])

								Totals by Heater Hole
NHH10	3.29+0.95 2.88±1.05	3.30+1.06 3.47±1.05	3.34+1.14 2.99±1.16	3.61+1.09 3.41±0.70	3.56+1.03 3.30±1.04	3.07+1.21 2.89±0.96	3.16+0.99 2.83±1.02	3.17±1.06
SHH5	3.27+0.97 2.87±1.00	2.61+1.06 3.04±1.06	3.02+1.04 3.05±0.91	3.20+1.13 3.28±0.91	3.22+0.99 3.28±1.06	2.73+1.04 3.36±0.99	2.85+0.74 3.02±1.06	3.05±1.02

*Table 3 gives key to arrangement of numbers

TABLE 6. Crack Measurements Close to Heater Hole
(Measurements are given by spot, for four different sections)

	2	4	6	8	10	12	14	16	18	20	22
Density (number/mm^2)											
NHH10PT-1	59	0	0	30		0	30	30		0	0
NHH10PT-6	59	30	119	59	237	148	89	59			
SHH5PT-1			0	326	0	59	30	59	59	30	0
SHH5PT-6				89	89	0		178	30	59	178
Average length (μm)											
NHH10PT-1	47	0	0	27	0	47	48	0	0		
NHH10PT-6	36	189	66	96	50	14	42	20			
SHH5PT-1			0	7	0	12	37	9	35	8	0
SHH5PT-6				14	49	0		14	28	113	34
Length density (mm/mm^2)											
NHH10PT-1	2.79	0	0	0.81	0	1.40	1.43	0	0		
NHH10PT-6	2.16	5.62	7.82	5.70	11.83	2.11	3.71	1.20			
SHH5PT-1			0	2.31	0	0.74	1.10	0.55	2.07	0.24	0
SHH5PT-6				1.29	4.33	0		2.57	0.84	6.73	6.07

TABLE 7. Modal Analyses (vol% of NHH10PT Samples)

	Average[1] Deuteric	NHH10PT				
		1	2	3	4	5
Plagioclase	42.85±1.08	46.1	36.5	43.8	37.4	56.4
K-Feldspar	17.97±0.82	17.3	21.9	23.7	25.2	18.2
Quartz	27.17±1.23	25.7	25.6	19.9	26.2	17.0
Biotite	5.38±0.53	5.6	8.9	6.3	3.0	3.6
Muscovite	1.48±0.28	1.8	2.9	1.7	2.5	0.6
Chlorite	0.99±0.18	1.3	1.6	2.0	1.9	1.4
Calcite	0.30±0.08	0.0	0.0	0.0	0.5	0.6
Czo/Ep	0.73±0.07	0.4	0.6	0.8	1.6	1.0
Titanite	0.44±0.10	0.6	0.4	0.5	0.3	0.4
Magnetite	0.78±0.10	1.1	1.1	1.0	1.0	0.5
Rutile	0.00	0.0	0.0	0.0	0.0	0.0
Pyrite	0.03±0.03	0.0	0.0	0.0	0.3	0.1
Accessories[2]	0.33	0.0	0.5	0.3	0.1	0.2

[1] Average of 19 deuterically altered samples from Connolly (1981).

[2] Allanite, Apatite and Zircon.

TABLE 8. Analyses of Feldspars from NHH10PT

Sample	K-Feldspar			Plagioclase		
	No. of Analyses	Avg.	S.D	No. of Analyses	Avg.	S.D.
NHH10PT-1	47	89.8	4.3	101	29.8	9.5
NHH10PT-2	60	89.7	5.5	97	31.3	13.8
NHH10PT-3	74	87.4	11.4	149	30.7	9.2
NHH10PT-4	67	89.9	5.9	87	30.6	9.2
NHH10PT-5	15	91.6	7/2	50	34.0	9.5
Average		89.7			31.3	
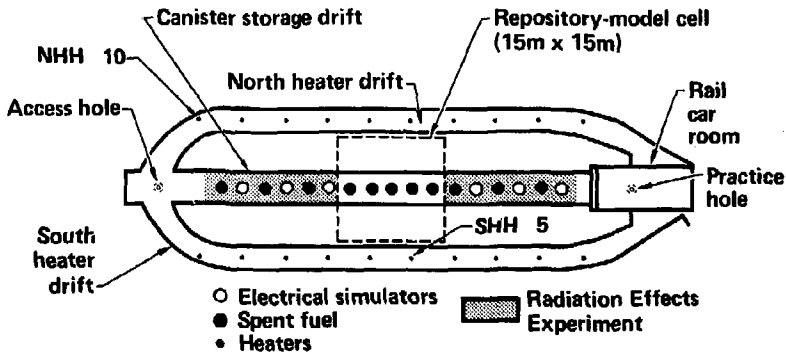
Fig. 1. Plan view of the layout of the SFT-C showing the principal features of the overall experiment. Material examined in this study was taken from the vicinity of heater drift boreholes NHH10 and SHH5.
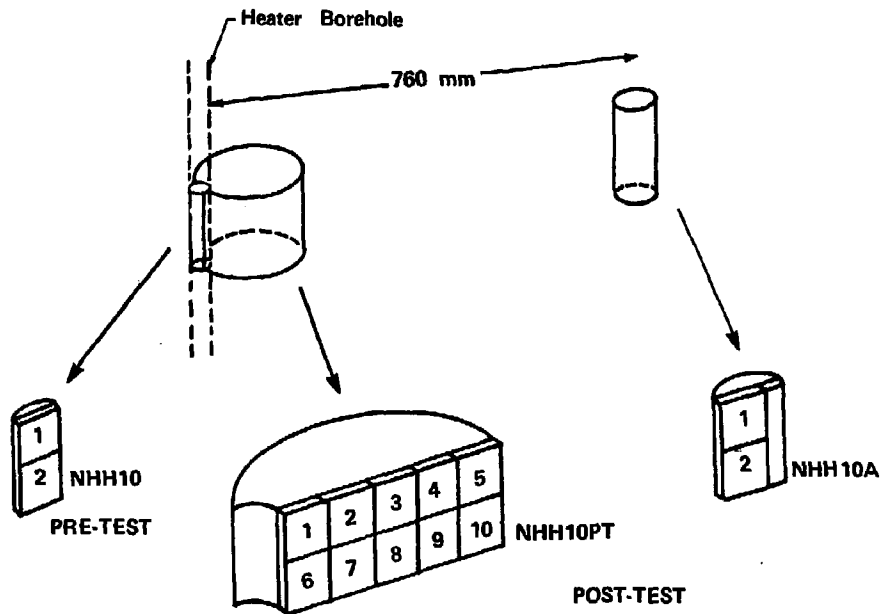
Fig. 2. Sketch showing the relative locations of sections examined and section labeling scheme. The arrangement here applies to NHH10, i.e., heater hole 10 in the north heater drift. It applies to south heater drift hole 5 if "SHH5" is substituted for "NHH10" in all labels and if sections SHH5A-1 and SHH5A-2 are interchanged. Core CHH5PT did not intersect the heater hole as did core NHH10PT.
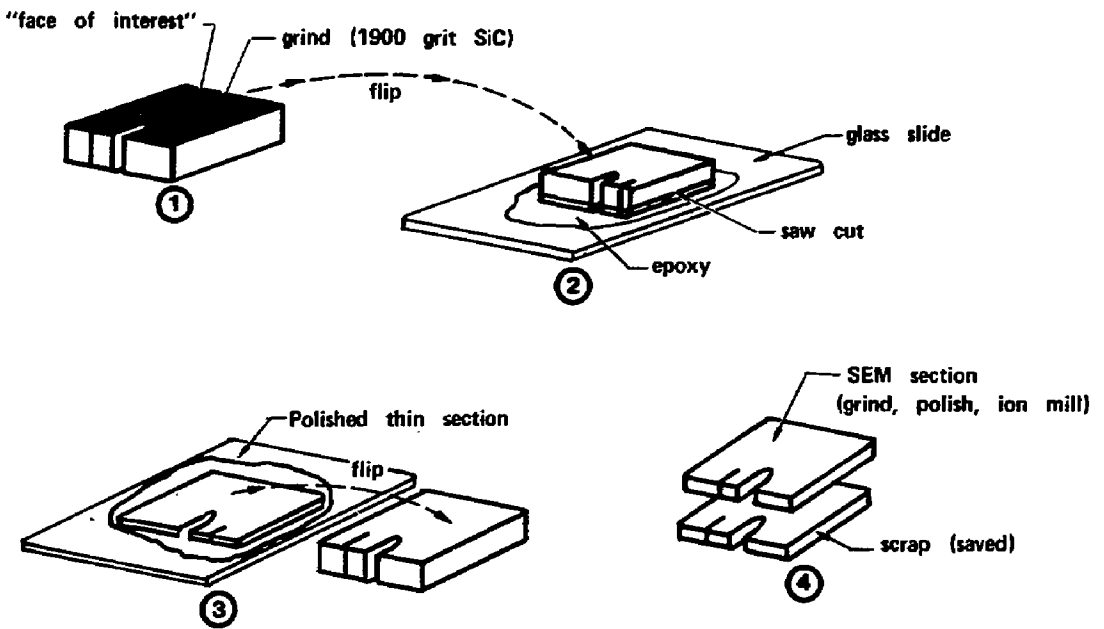
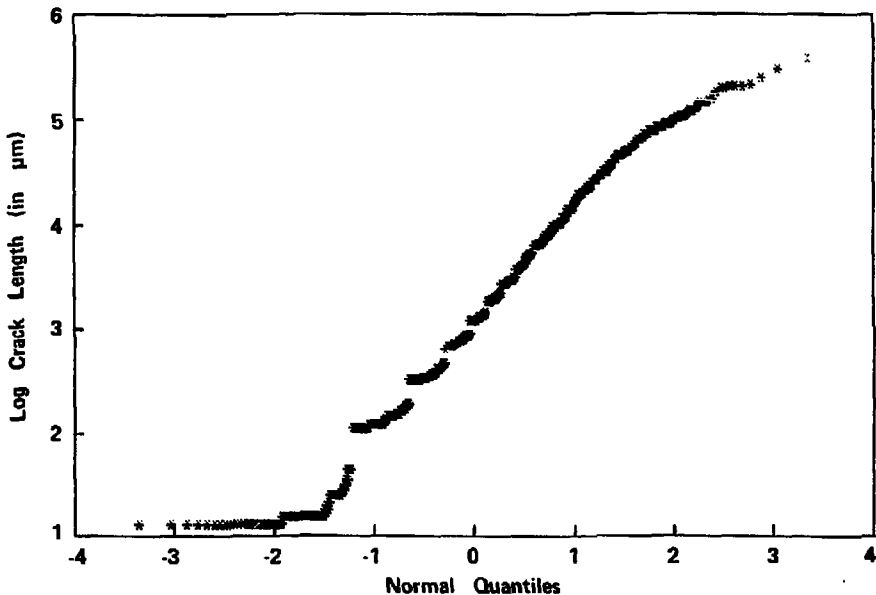Fig. 3. Steps in sample preparation of sections for SEM and OM analysis.

Fig. 4. Quantile-quantile (QQ) plot of log length of all 1245 cracks counted, demonstrating by its linearity the log-normal distribution of those lengths. The bottom end of the QQ plot is pushed up by a round-off error in digitization which forces all perceived cracks to have a minimum length of about 3μm. The top end is suppressed by truncation of long cracks at the edges of the photograph.
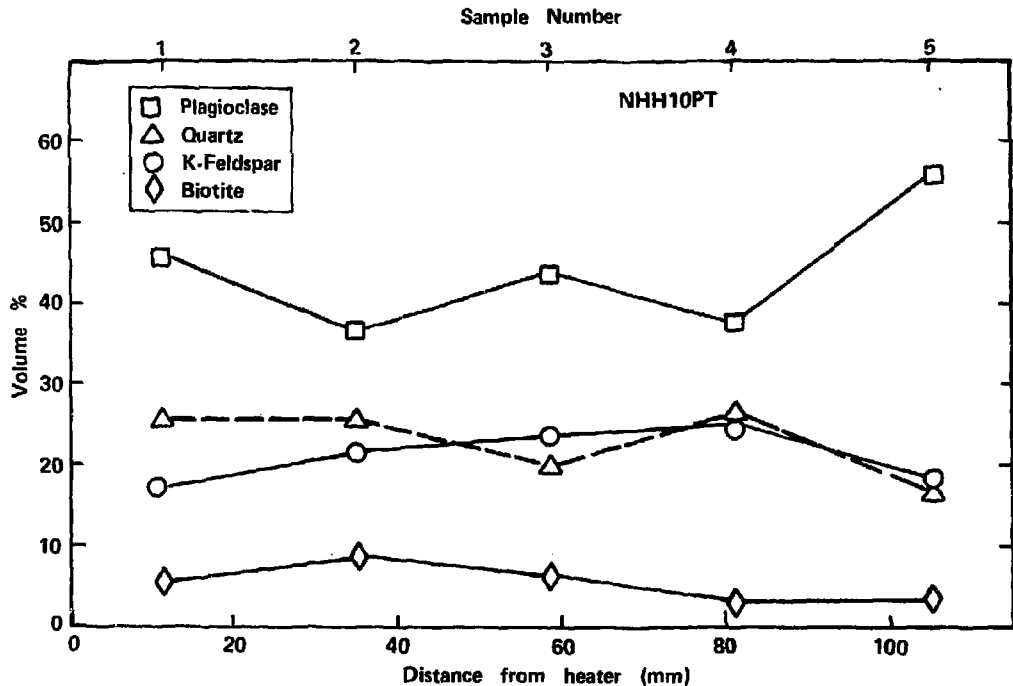
Fig. 5. Modal abundances of plagioclase, K-feldspar, quartz and biotite in NHH10PT samples relative to the heater.
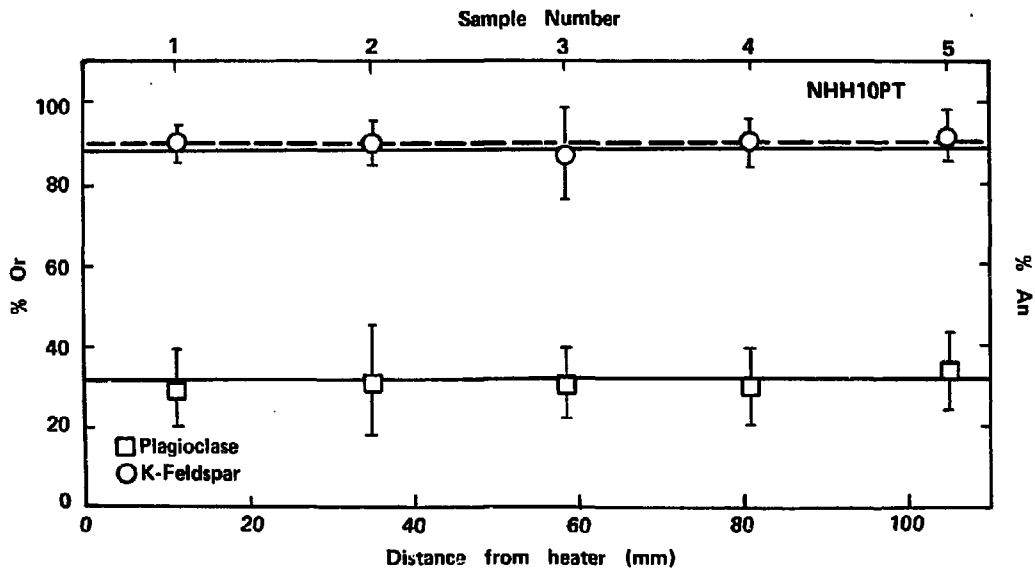
Fig. 6. Variation in feldspar compositions in NHH1OPT samples relative to the heater. Dashed lines are the average compositions from NHH1OPT samples, and solid lines are the average of all pre-test samples (Patrick et al., 1984).